Thermal Stability of Supercapacitor for Hybrid Energy Storage System in Lightweight Electric Vehicles: Simulation and Experiments

Vima Mali and Brijesh Tripathi

Abstract—Recent research findings indicate that the non-monotonic consumption of energy from lithium-ion (Li-ion) batteries results in a higher heat generation in electrical energy storage systems. During peak demands, a higher heat generation due to high discharging current increases the temperature from 80 °C to 120 °C, thereby resulting in thermal runaway. To address peak demands, an additional electrical energy storage component, namely supercapacitor (SC), is being investigated by various research groups. This paper provides insights into the capability of SCs in lightweight electric vehicles (EVs) to address peak demands using the worldwide harmonized light-duty driving test cycle (WLTC) driving profile in MATLAB/Simulink at different ambient temperatures. Simulation results indicate that temperature imposes a more prominent effect on Li-ion batteries compared with SCs under peak demand conditions. The effect of the discharging rate limit on the Li-ion battery current is studied. The result shows that SCs can accommodate the peak demands for a low discharging current limit on the battery, thereby reducing heat generation. Electrochemical impedance spectroscopy and cyclic voltammetry are performed on SCs to analyze their thermal performance at different temperatures ranging from 0 °C to 75 °C under different bias values of −0.6, 0, 0.6, and 1 V, respectively. The results indicate a higher specific capacitance of the SC at an optimum operation temperature of 25 °C for the studied bias. This study shows that the hybrid combination of the Li-ion battery and SC for a lightweight EV can address peak demands by reducing thermal stress on the Li-ion battery and increasing the driving range.

Index Terms—Electric vehicle, lithium-ion battery, supercapacitor, thermal stability.

I. INTRODUCTION

AN alternative emission-free technology in the transportation sector is the priority of every government, as it can reduce urban air pollution and greenhouse gas emissions [1]. Hence, the use of electric vehicles (EVs) may be the best solution to reduce global warming [2]. Lightweight battery-powered EVs may afford the greatest CO_2 emission reduction by 87.3% compared with the baseline value of 2050 [3]. Different models for analyzing the energy storage systems of EVs have been proposed recently. An optimal robust model has been proposed for the short-term scheduling of distribution networks to render EV parking as an energy storage system with uncertainties [4]. By adopting a particle swarm optimization algorithm, the demand response programs and smart charging/discharging of plug-in EVs have been investigated to improve the reliability of radial distribution systems [5]. An optimal stochastic scheduling model has been proposed for power sharing from NaS batteries with combined heat and power units [6]. The energy management strategy of a parallel hybrid EV equipped with a battery and supercapacitor (SC) in a hybrid electrical energy storage system (EESS) has been reported recently [7]. Reference [8] provides a comprehensive review of energy management strategies for the hybrid energy storage systems of EVs. Among the energy storage devices, lithium-ion (Li-ion) batteries are widely used for energy storage because of their high energy density and light weight [9]. Different risks are associated with the Li-ion batteries when they are exposed to the overcharging, high ambient temperature, etc. The onset of an exothermic chemical reaction can cause severe losses of property and life [10].

Despite these risks, Li-ion batteries are becoming the integral part of lightweight EVs, which generally weigh less than 100 kg and are smaller than conventional commercial vehicles propelled by an electric motor instead of a conventional internal combustion (IC) engine. In EVs, the electric motor is powered by the Li-ion battery based EESS. Recent research findings indicate that the non-monotonic consumption of energy from Li-ion batteries result in a higher heat generation owing to the high discharging rate in the EESS [11]. If the generated heat increases the temperature from 80 °C to 125 °C, thermal runaway will occur [12]. Various power management strategies for the hybrid energy storage system are proposed and compared [13] to protect the primary power source from sudden high-power load transients. An effective energy management control method with an adaptive rate limiter is proposed to protect the primary source [14]. The reported control algorithms do not consider the charging and discharging rate limit patterns of the battery be-

cause the battery might be affected by thermal runaway and cell rupture if overheated or overcharged. In extreme cases, this can result in combustion. The battery reference current, duty ratio, and power are controlled by the proportional-integral (PI) control parameters (K_p and K_i) because these parameters govern the output [15]. SCs should be able to operate at a wide range of temperatures to be applied commercially. Limited data are available regarding the thermal stability of SC, wherein thermal characterization has been performed at a constant ambient temperature [16]. However, the optimum operation temperature of SCs under different biases has not been investigated sufficiently, to determine their feasibility, as one of the components in the hybrid EESS of EVs with different battery discharging current limits. Hence, this study addresses this gap and can be segmented into two parts. In the first part, the thermal performance of the SC is analyzed based on theoretical simulation by limiting the battery discharging current rate in the hybrid EESS, comprising an SC and Li-ion battery, for a lightweight EV in MATLAB/Simulink. In the second part, the electrochemical characteristics of the SC are presented to experimentally investigate the optimum operation temperature with respect to different biases. The results obtained in terms of specific capacitance and equivalent series resistance (ESR) are explained.

II. THEORETICAL DESCRIPTION OF SIMULATION MODEL

A. Power Management Strategy of EESS

Many different topologies regarding hybrid combinations of the Li-ion battery and SC for EVs have been reported [17]-[19]. However, each of these topologies has their own advantages and limitations. In this study, a MATLAB/Simulink model based on the parallel active topology in the hybrid EESS for EV applications is developed using conventional direct current (DC) boost and buck/boost DC/DC converters. In this theoretical model, the SC (16 V, 500 F) and Li-ion battery (12.8 V, 40 Ah) are connected in parallel via a bidirectional buck/boost converter and a unidirectional boost converter to maintain a voltage of 42 V in the DC link (V_{DC}). This is performed to analyze the behaviors of SCs considering peak demands in the standard driving cycle at different temperatures ranging from 0 °C to 75 °C and to estimate the driving range. In the hybrid EESS, the power allocation is performed considering the calculated power at the wheels from the predefined driving cycle, quality of road, ambient temperature, air density, converter efficiency, etc. For the efficient utilization of the Li-ion battery and SC in the EESS, an appropriate power-split management strategy is necessitated, involving predefined rules based on prior knowledge of the driving profile. The power at the wheels is key for identifying different modes of operation such as regenerative braking, acceleration, and normal modes. A flowchart of the control strategy is shown in Fig. 1, where P_W is the power required at the wheels; SOC_{SC} is the state of charge (SOC) of SC; $SOC_{SC,\max}$ and $SOC_{SC,\min}$ are the maximum and minimum values of the SOC of SC, respectively; $VSC_{\max}$ and $VSC_{\min}$ are the maximum and minimum voltages across the terminals of SC, respectively; $P_{batt,\max}$ is the maximum power of Li-ion battery; A is the connector; $P_{SC}(sto)$ is the power stored in SC; and $P_{SC}(del)$ is the power delivered by SC.
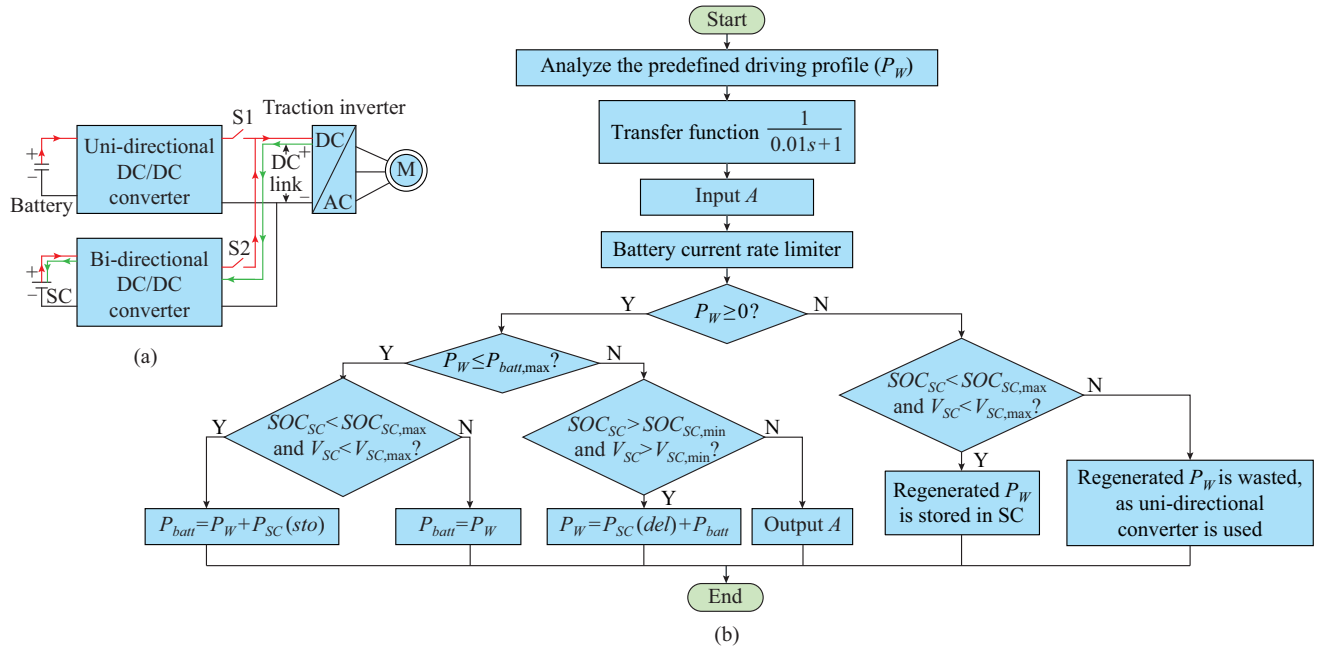

Fig. 1. Topology of hybrid EESS and power management strategy. (a) Parallel active topology of hybrid EESS. (b) Flow chart of power management strategy.

Two sources are controlled by a switching strategy that is designed to satisfy the power demands at the wheels. The description logic of switching algorithm is explained in Table I. Switches S1 and S2 are connected across the Li-ion battery and the SC. In the power management strategy, the predefined driving profile, i.e., P_W is firstly analyzed at any par-

ticular instant. Secondly, P_W is fed to the transfer function relating the output or response of a system such as a filter circuit, to the input or stimulus. The reference currents generated from the driving profile are compared with the actual currents drawn from the battery by the controller for generating pulse width modulation (PWM) signals. These signals enable the controller to operate in either the buck or boost mode. A similar strategy has been reported in [20]. With respect to the driving profile, the stored capacity of the hybrid EESS is analyzed at every instant in terms of ampere-hour, SOC, and voltage. An economic optimization analysis considering the cost of SC and Li-ion battery has been presented in [21] for lightweight EV.

TABLE I
SWITCHING CHARACTERISTIC REFERRING TO PARALLEL ACTIVE TOPOLOGY
OF HYBRID EESS IN FIG. 1

| Case | Switching state | | Condition | Mode |
	Battery (S1)	SC (S2)		
SS1	0	0	Off operation	No operation
SS2	1	0	Battery is high, SC is low	Normal
SS3	0	1	Battery is low, SC is low	Regenerative braking
SS4	1	1	Battery is high, SC is high	Acceleration

In the parallel active topology of the hybrid EESS shown in Fig. 1, switch S1 is connected across the Li-ion battery, and switch S2 is connected across the SC with relays. These relays operate based on the power demands at the wheels at any particular time instant as well as the available battery capacity and SC capacity.

B. Calculation of Driving Range

The driving range of an EV depends on several parameters such as its characteristics, driving profile, and the storage capacity of the hybrid EESS. The parameters of the EV [22]-[25] considered in the simulation are listed in Table II.

TABLE II
SIMULATION PARAMETER OF HYBRID EV

Parameter	Value
Vehicle mass M	50 kg
Rolling resistance coefficient C_{rr}	0.01
Gravity acceleration g	9.8 m/s^2
Inclination angle θ	0
Drag coefficient C_d	0.9
Vehicle frontal area A_f	0.5 m^2
Electronic efficiency $\eta_{converter}$	0.98
Motor efficiency η_{motor}	0.95
Efficiency of mechanical drive train $\eta_{drive,train}$	0.90
Initial battery energy	512
Base load of front light	35.0 W
Base load of back light	12.0 W
Base load of side light lamp	11.7 W

The total required power at the wheels P_W for an EV can be calculated as [26]-[28]:

$$P_W = P_{base} + P_{roll} + P_{drag} + P_g + P_{acc} \qquad (1)$$

where P_{base} is the power requirement of the front light, back light, and side light lamp; P_{roll} is the power of the rolling resistance; P_{drag} is the power required to overcome the aerodynamic drag; P_g is the power required to align the vehicle against gravity; and P_{acc} is the acceleration or braking power. The dominant components are P_{drag} and P_{acc}.

From the average power consumption at the wheels at every instant expressed in (1), the average energy consumption at the wheels E_W over the driving cycle can be calculated by integrating the total power with respect to time as:

$$E_W = \int_0^T P_W dt \qquad (2)$$

where T is the total driving time.

The driving range R can be calculated as:

$$R = \frac{E_{EESS} D}{E_W} \qquad (3)$$

where E_{EESS} is the initial stored electrical energy in the hybrid system; and D is the distance included in the driving cycle.

The available initial energy of E_{EESS} is calculated as:

$$E_{EESS} = \eta \left(\Delta SOC_{batt} \cdot E_{int,batt} + \Delta SOC_{SC} \cdot E_{int,SC} \right) \qquad (4)$$

$$\eta = \eta_{converter} \eta_{motor} \eta_{drive,train} \qquad (5)$$

where η, $\eta_{converter}$, η_{motor}, and $\eta_{drive,train}$ are the efficiencies of the EV traction system (i.e., 83.79%), electronic, motor, and mechanical drive train, respectively; ΔSOC_{batt} and ΔSOC_{SC} are the SOC of the Li-ion battery and SC change from the beginning to the end in a complete driving cycle, respectively; and $E_{int,batt}$ and $E_{int,SC}$ are initial energy of the the Li-ion battery and SC, respectively. Using this theory, the driving range of EVs can be estimated for various temperature conditions in the city.

III. EXPERIMENTAL DETAIL

To use SCs in transportation applications, the electrical and thermal behaviors of SCs in an operation environment must be understood [29]. SCs are a class of electrochemical capacitors with a high capacitance and are composed of two high-surface-area porous electrodes soaked in an ionic electrolyte. The two electrodes are generally separated by a porous structure, which prevents electrical short circuit while permitting the movement of ions [30]. The universally used equivalent electrical circuit model of the SC with the Warburg element is shown in Fig. 2, where the ideal element C_P is the parallel capacitance with the Warburg coefficient; R_P is the parallel resistance; R_S is the series resistance; and L is a series inductor.
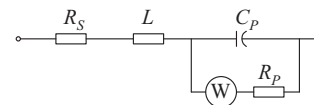

Fig. 2.   Equivalent electrical circuit model of SC.

The series resistance R_S is typically known as ESR, which represents the energy loss during the charging and discharging process. The parallel resistance R_P is the pathway for electrical energy loss in the SC during its self-discharging. In a practical SC, R_P is always significantly higher than R_S. The series inductor L is typically extremely small and results from the physical construction of the SC. The values of the elements of the equivalent circuit model can be determined using Gouy and Chapman's theories [30], [31]. In recent years, interests have increased regarding SCs containing redox-active electrolytes that can offer additional capacitance as a strategy to improve the overall storage performance of the EESS [32].

Electrochemical impedance spectroscopy (EIS) has been performed on the SC based on different ambient temperatures and voltage biases, as shown in Supplementary Materials. EIS analyzes the effect of frequency on the ESR and specific capacitance [33] with respect to different bias voltages. Various energy storage devices have been investigated using EIS techniques, e. g., batteries and SCs. EIS is a well-known technique for analyzing aging based on the ESR and capacitance [34]. EIS provides a deeper insight into the internal processes of a system by analyzing the impedance characteristics under a broad range of frequencies. This is performed by injecting a small sinusoidal voltage signal (10 mV) into the device and measuring the response current, or vice versa (galvanostatic and potentiostatic approaches) [35]. In this study, the electrochemical characteristics of an SC (2.7 V, 10 F) are investigated at different temperatures with respect to different bias voltages, and the experimental results are presented. EIS measurements have been performed for the SC in the frequency range of 1 Hz to 5 kHz using a Metrohm-Autolab equipment (PGSTAT302N). The thermal performance of an SC has been characterized experimentally based on a typically used approach [36]. For its thermal characterization, a constant temperature has been achieved by storing the SC inside a heating chamber filled with an insulating thermic fluid. The temperature of the heating chamber has been varied by placing it on a proportional integral derivative (PID) controlled hot plate. The fluid temperature is recorded by installing a digital thermometer sensor inside the chamber. The EIS and CV experiments are performed on the SC by varying the temperatures to 0, 25, 50, and 75 °C at constant bias voltages of −0.6, 0, 0.6, and 1 V, respectively.

IV. RESULTS AND DISCUSSION

A. Driving Profile of EV

The first step in calculating the range of any EV is to select the driving profile. Many countries and organizations have developed driving cycles to analyze the performance of vehicle emissions, traffic impact, and fuel consumption. A worldwide harmonized light-duty driving test cycle (WLTC) is considered for this study. The WLTC is launched by the World Forum for the Harmonization of Vehicle Regulations (WP. 29) by the United Nations Economic Commission for Europe [37].

As shown in Fig. 3, from the WLTC driving cycle (240 s), the average running speed of the vehicle is 29.3 km/h, the highest speed is 56.7 km/h, and the distance is 1.953 km.
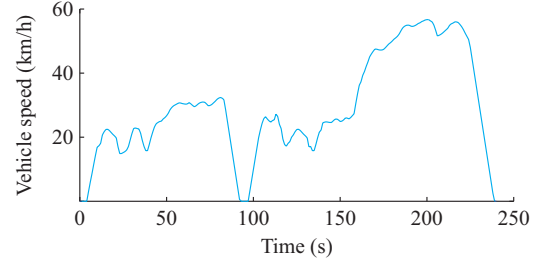

Fig. 3. WLTC driving profile.

B. Required Power at Wheels with Respect to Temperature

Figure 4 shows the effect of the ambient temperature on the total required power at the wheels, which is calculated using (1). The variation in air density with the change of temperature, as shown in Table III, affects the required power at the wheels P_W. Figure 5 shows that the required power at the wheels is the lowest at the highest temperature owing to the lowest drag resistance provided by air. At 0 °C, the drag resistance increases, thereby increasing the required power. The negative power (acceleration) in the driving profile indicates that brakes are applied.
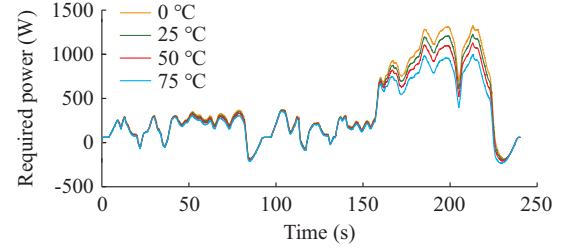

Fig. 4. Required power at wheels P_W considering driving profile and temperature.

TABLE III
AIR DENSITY VARIATION WITH RESPECT TO TEMPERATURE

Temperature (°C)	Air density (kg/m³)
0	1.290
25	1.171
50	1.047
75	0.882

C. Temperature Effect on Li-ion Battery in Hybrid EESS

The hybrid combination (Li-ion battery and SC) is used to deliver the required power at the wheels under various temperature conditions. The variation in the Li-ion battery output at different temperatures significantly affects its performance, life, and reliability. Hence, thermal management strategies must be developed to ensure that the batteries operate well at subzero temperatures [38]. As shown in Fig. 5(a), for a low battery discharging current limit, the battery partially supplies the required power at the wheels. As the battery discharging current limit increases, the required power at the

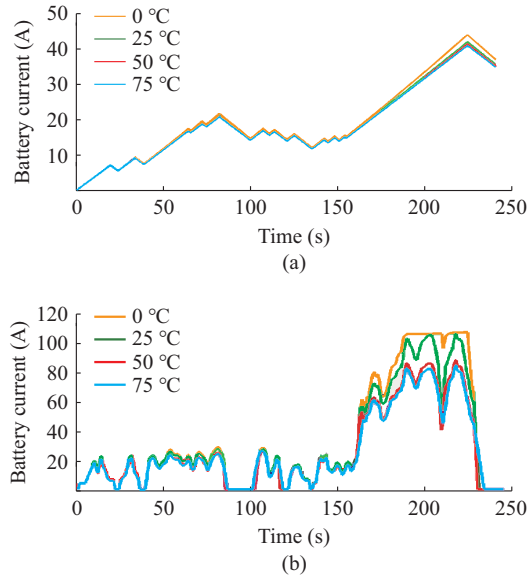wheels is primarily satisfied by the battery at higher temperatures above 0 °C, as shown in Fig. 5(b).

Fig. 5.   Temperature effect on battery current in hybrid EESS. (a) Low battery discharging current limit. (b) High battery discharging current limit.

Furthermore, Fig. 5(b) shows that as the temperature decreases, the current drawn from the Li-ion battery increases and the battery capacity decreases. Because of the colder environment, there is a slower chemical process that significantly reduces the supply capacity of the Li-ion battery and increases the internal resistance simultaneously. The temperature of the battery during charging and discharging is one of the key factors that affect the performance and the lifespan of the Li-ion battery. The thermal runaway of a single cell can cause a chain reaction with other cells, potentially causing fire and losses of life and property [39]. From Fig. 5(b), it is observed that a higher power is required from 150 to 240 s at 0 °C; however, the Li-ion battery could not supply the required power during the peak requirement. Researchers have reported the poor performance of Li-ion batteries under severe climatic conditions [40], which encourages the development of heating methods to reduce the deterioration of Li-ion batteries as well as enhance their performances. Accurate information regarding the SOC is crucial for extracting the maximum performance safely from Li-ion batteries. The effect of temperature on SOC is non-negligible. As expected, a lower discharging current limit decreases the battery discharging rate, as shown in Fig. 6(a), whereas a higher discharging limit results in a faster battery discharging rate (as shown in Fig. 6(b)). The SOC of battery remains at approximately 97% after 240 s under a lower discharging current limit, whereas it reaches approximately 94% for a higher discharging current limit.

D. Effect of Temperature on SC in Hybrid EESS

It is crucial to manage the battery charging with respect to the temperature, as described in Section IV-C. SCs are the most promising energy storage devices to manage the charging of batteries and enhance their lifetime [41]. Regenerative braking can be identified in Fig. 7 by the negative current

values. The effect of a lower current discharging limit on the Li-ion battery is observed on the SC discharging current. For a low discharging current limit on the battery, the required power at the wheels is primarily satisfied by the SC because the current profile drawn from the SC (Fig. 7(a)) closely matches with the required power shown in Fig. 4. As the battery discharging current limit increases, the SC supplies power only in the case of peak demands and stores the power for peak regeneration (as shown in Fig. 7(b)). This result indicates that the use of the SC will be more efficient if the battery discharging current limit is lower, which ensures a greater energy storage in the SC during the regeneration. Meanwhile, Figure 7(b) shows that the power drawn from the SC is high at the beginning, implying that the high power requirement (i.e., high charge and discharge rates) is supported by the SC over a wide range of temperatures. The SC reduces the stress on the primary source, thereby increasing the lifespan of the overall system. This justifies the importance of SCs in EV applications.
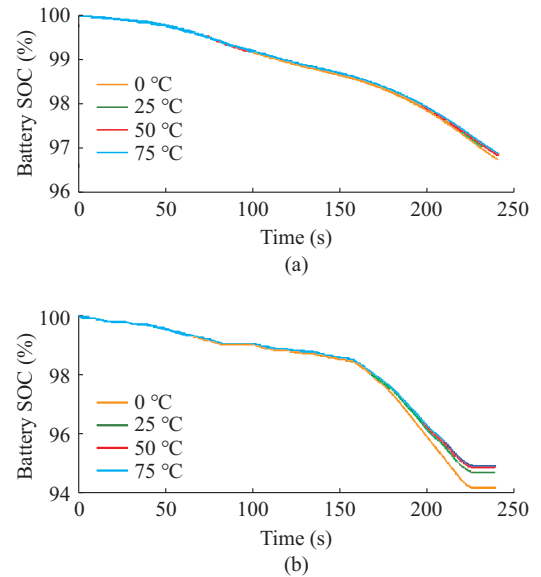

Fig. 6.   Temperature effect on battery SOC in hybrid. (a) Low battery discharging current limit. (b) High battery discharging current limit.

Figure 8 shows the SOC of SC decreases and increases because of the utilization of the SC during peak demands and the storage of additional energy due to regenerative braking, respectively. A lower battery discharging current limit results in a faster discharging of the SC (as shown in Fig. 8(a)), whereas a higher current discharging limit of the battery reduces the requirement from the SC and increases the SOC of the SC because of the regenerative braking (as shown in Fig. 8(b)).

E. Calculation of Driving Range with and Without SC

The driving range of hybrid EVs is calculated for 240 s of the driving cycle and then repeated for the 3600 s cycle. The driving range increases with the temperature in the Li-ion battery-based EESS as shown in Fig. 9. A hybrid EESS combination of Li-ion battery and SC improves the driving range by approximately 3.5% for the complete range of temperature owing to the additional energy supplied by the SC.
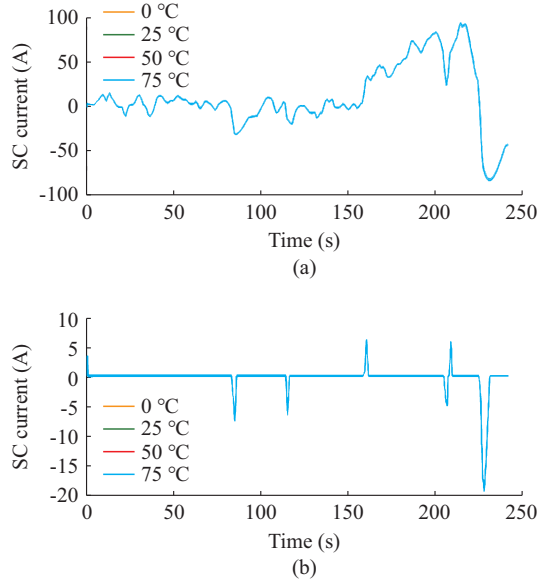
Fig. 7. Effect of temperature on SC current in hybrid EESS. (a) Low battery discharging current limit. (b) High battery discharging current limit.
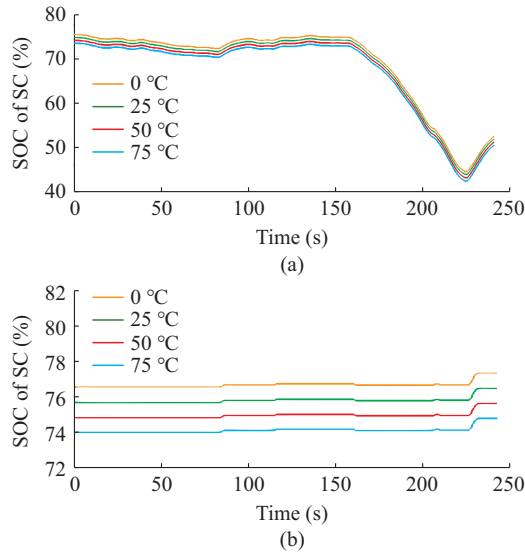

Fig. 8. Effect of temperature on SOC output of SC in hybrid EESS. (a) Low battery discharging current limit. (b) High battery discharging current limit.
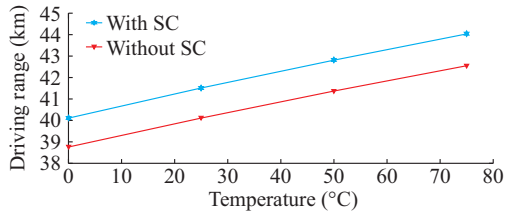

Fig. 9. Driving range of EVs using hybrid EESS with respect to temperature after 3600 s of driving.

Using the hybrid EESS, the driving range is affected by the temperature. At sub-zero temperatures, the available output energy of the battery decreases, and the battery degrades because of Li plating, which results in an increase in the system operation cost and replacement cost. Range anxiety is a

key factor affecting the willingness of consumers to adopt EVs. Hence, it is concluded that the driving range depends significantly on the temperature. The improvement in the driving range is attributed to the additional energy stored in the SC (17.78 Wh) along with the available energy stored in Li-ion battery (512 Wh).

F. Effect of Temperature on Impedance Spectra of SC

EIS is the most robust technique among various electrochemical techniques used to measure the complex impedance and capacitive behavior of electrochemical cells such as batteries and SCs. The dynamic behavior of the electrochemical impedance spectra of SC is assessed in the frequency range from 1 Hz to 100 Hz at various temperatures and voltage biases. During the operation of the vehicle, the temperatures and voltages of the SCs would change. Figure 10 represents the Nyquist plot of SCs in the temperature range from 0 °C to 75 °C for various bias voltages of −0.6, 0, 0.6, and 1 V, respectively. The results indicate that the ESR of the SC is the minimum at approximately 25 °C, i. e., at 0.095 Ω for various biases investigated in this study. Hence, a reduced amount of energy is dissipated in the charging and discharging of the SC even at higher currents. At 0 °C, the ESR increases slightly owing to the slow motion of ions at the lower temperature. The increase in the ESR of the SC at sub-zero temperatures is negligible compared with the temperature effect observed on the Li-ion battery, as described in Section IV-C.
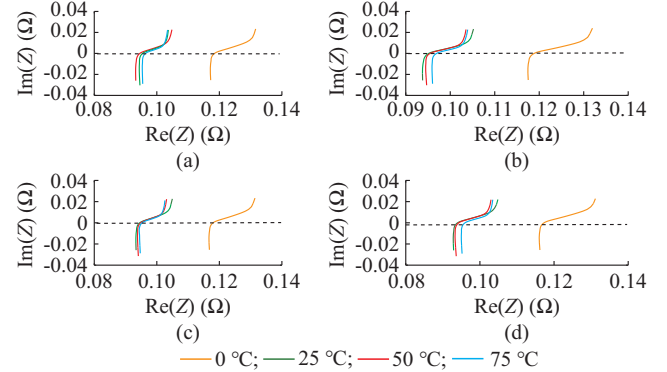

Fig. 10. Nyquist plot obtained using Autolab NOVA software for SC. (a) Bias voltage of −0.6 V. (b) Bias voltage of 0 V. (c) Bias voltage of 0.6 V. (d) Bias voltage of 1 V.

G. Effect of Temperature on Capacitance Spectra of SC

The performance of SC is analyzed in terms of storage capacity with respect to various temperatures. Figure 11 shows the SC capacitance variation with respect to different frequencies under different biases.

The stored electrical energy E in the SC is expressed as:

$$E = \frac{CV^2}{2} \tag{6}$$

where C is the capacitance of the SC; and V is the voltage across the terminals of the SC.

Subsequently, the capacitance of the SC is analyzed using the complex impedance Z obtained from the Nyquist plot of Fig. 11, and is expressed as:
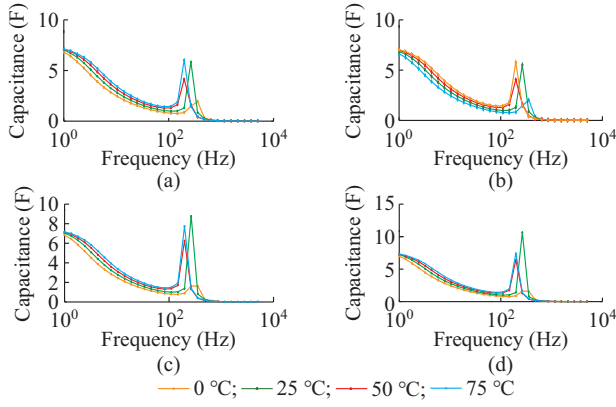
Fig. 11.   Bode plot obtained for capacitance versus frequency. (a) Bias voltage of −0.6 V. (b) Bias voltage of 0 V. (c) Bias voltage of 0.6 V. (d) Bias voltage of 1 V.

$$C = \frac{1}{j\omega \mathrm{Im}(Z(\omega))} \qquad (7)$$

where ω is the angular frequency; and $\mathrm{Im}(Z(\omega))$ is the imaginary part of $Z(\omega)$.

Figure 11 shows the dependence of capacitance on frequency in the temperature range from 0 ℃ to 75 ℃. The capacitance of the SC (i.e., storage capacity) remains high at higher temperatures in the frequency range from 1 to 100 Hz, but diminishes at lower temperatures. An anomalous peak is observed from 200 to 400 Hz, and it increases the bias; however, that phenomenon is inexplicable. At higher frequencies, the storage capacity of the SC remains constant (as evident from (6) and (7)) owing to the diffusion process in the SC that yields an impedance known as the Warburg impedance as shown in Fig. 2. At higher frequencies, the Warburg impedance in the SC is small, and the diffusing reactants do not propagate far. At lower frequencies, the reactants diffuse further, thereby increasing the Warburg impedance. As the temperature decreases, the conductivity of electrolytes remains low and obstructs the ion transport, thereby affecting the ion absorption/desorption in the electrical double layers of the SC. An increase in the temperature decreases the electrolytic viscosity but increases the reachability of the surface ions. Hence, the ions penetrate the respective electrodes and reaches deeper into them in a shorter time interval. This increases the pathway and reduces the ESR as the capacitance increases with respect to the temperature owing to increased ionic mobility at higher temperatures.

H. Effect of Temperature on Cyclic Voltammetry (CV) of SC

CV is the most effective and popular electrochemical technique employed to investigate the reduction and oxidation processes of molecular species. CV is performed on the SC at scan rates of 5 to 180 mV/s with respect to different temperatures in the range from 0 ℃ to 75 ℃. The results indicate that the shape of the CV curves is preserved even at higher scan rates, implying a fast charging transfer mechanism from the electrochemical double layers. The specific capacitance of the SC [42], [43] is calculated as:

$$C = \frac{A}{\Delta v \dfrac{\partial v}{\partial t} m} \qquad (8)$$

where A is the area under the CV curve; Δv is the potential window; m is the mass of the SC; and $\partial v/\partial t$ is the scan rate.

Figure 12 shows the variation in the ESR extracted from the impedance measurements as a function of temperature. The values of the specific capacitance extracted from the CV curve are listed in Table IV. A high specific capacitance of 56.65 F/g is observed at 25 ℃ for all the bias voltages investigated at a low scan rate of 5 mV/s. A higher specific capacitance is observed at a lower scan rate. This is because at lower scan rates, the ions can penetrate the pores of the material, whereas at higher scan rates, the ions do not have sufficient time and hence remain on the outer surface. At 25 ℃, a better performance is observed for the SC.
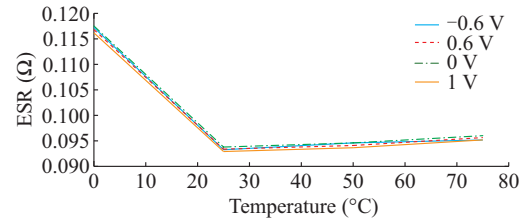

Fig. 12.   Variation in ESR with respect to temperature and bias voltage.

TABLE IV
VALUE OF SPECIFIC CAPACITANCE EXTRACTED FROM CV CURVE

Temperature (℃)	C (F/g)	
	Scan rate of CV is 5 mV/s	Scan rate of CV is 180 mV/s
0	48.82	4.27
25	56.65	4.82
50	47.20	4.41
75	45.25	3.97

In general, the main findings from this study regarding a hybrid EESS comprising the Li-ion battery and SC are as follows.

1) The simulation results indicate the excellent performance of the SC during peak demands and at various temperature conditions, whereas the capacity of the Li-ion battery decreases significantly with the temperature.

2) A low discharging current rate limit on the battery results in the slow discharging of the battery, and most of the power requirement is fulfilled by the SC. However, a high discharging current rate limit on the battery results in a faster discharging of the battery.

3) The SC is investigated experimentally using EIS and CV at various bias voltages of −0.6, 0, 0.6, and 1 V, respectively. At the temperature of 0 ℃, the ESR increases slightly to 0.119 Ω. A high specific capacitance of 56.65 F/g is observed at 25 ℃ for the bias voltages investigated. The experimental results indicate that the SC possesses a higher specific capacitance at an optimal operation temperature of 25 ℃ for all the investigated biases, signifying that the bias imposes the a less significant effect on the SC performance with respect to the temperature.

4) This study demonstrates that the SC can be used in combination with Li-ion batteries in the hybrid EESS of a

lightweight EV to address peak demands, reduce thermal stress on the primary source (Li-ion battery), and increase the driving range. An increase of 3.5% in the driving range is obtained when using both the SC and Li-ion battery compared with that without using the SC, which is obtained owing to the additional energy provided by the SC.

V. Conclusion

During peak demands, a higher heat generation increases the temperature of Li-ion batteries, thereby causing thermal runaway. To address peak demands, an additional electrical energy storage component, namely SC, is used in this study. The thermal stability of the SC in a hybrid combination is investigated for a WLTC driving profile in MATLAB/Simulink at various temperatures in the range from 0 °C to 75 °C. The results indicate the excellent thermal stability and peak demand handling capacity of the SC, thereby supporting the use of the SC as a hybrid combination for the secondary source. A low discharging current rate limit on the battery results in a slow discharging of the battery, and most of the power requirement is fulfilled by the SC. However, a high discharging current rate limit on the battery results in a faster discharging of the battery. The simulation shows that a 3.5% higher driving range can be obtained using an SC in addition to a Li-ion battery for 1 hour of driving under assumed conditions. EIS and CV studies pertaining to the SC demonstrate excellent performances for the temperature range investigated. For the studied bias voltages of −0.6, 0, 0.6 and 1 V, a low ESR value of 0.095 Ω is observed at 25 °C. Subsequently, as the temperature decreases approximately 0 °C, the ESR increases slightly to 0.119 Ω for all the biases investigated. The specific capacitance of 56.65 F/g remains high at 25 °C for a scan rate of 5 mV/s compared with that of 180 mV/s. Moreover, the results indicate that the bias voltage does not significantly affect the SC. This study demonstrates that SCs can be used in combination with Li-ion batteries in the hybrid EESS of a lightweight EV to address peak demands.

References

[1] C. Fernández-Dacosta, L. Shen, W. Schakel *et al.*, "Potential and challenges of low-carbon energy options: comparative assessment of alternative fuels for the transport sector," *Applied Energy*, vol. 236, pp. 590-606, Feb. 2019.

[2] G. Hill, O. Heidrich, F. Creutzig *et al.*, "The role of electric vehicles in near-term mitigation pathways and achieving the UK's carbon budget," *Applied Energy*, vol. 251, pp. 113111, Oct. 2019.

[3] J. C. G. Palencia, Y. Otsuka, M. Araki *et al.*, "Impact of new vehicle market composition on the light-duty vehicle fleet CO_2 emissions and cost," *Energy Procedia*, vol. 105, pp. 3862-3867, May 2017.

[4] M. Ghahramani, M. Nazari-Heris, K. Zare *et al.*, "Energy management of electric vehicles parking in a power distribution network using robust optimization method," *Journal of Energy Management and Technology*, vol. 2, no. 3, pp. 22-30, Sept. 2018.

[5] O. Sadeghian, M. Nazari-Heris, M. Abapour *et al.*, "Improving reliability of distribution networks using plug-in electric vehicles and demand response," *Journal of Modern Power Systems and Clean Energy*, vol. 7, no. 5, pp. 1189-1199, Sept. 2019.

[6] M. Nazari-Heris, S. Madadi, S. Abapour *et al.*, "Optimal stochastic scheduling of virtual power plant considering NaS battery storage and combined heat and power units," *Journal of Energy Management and Technology*, vol. 2, no. 3, pp. 1-7, Sept. 2018.

[7] A. S. Kahnamouei, T. G. Bolandi, and M. R. Haghifam, "The concep-

[8] A. Geetha and C. Subramani, "A comprehensive review on energy management strategies of hybrid energy storage system for electric vehicles," *International Journal of Energy Research*, vol. 41, no.13, pp. 1817-1834, Oct. 2017.

[9] Y. Liang, "A review of rechargeable batteries for portable electronic devices," *InfoMat*, vol. 1 no. 1, pp. 6-32, Mar. 2019.

[10] L. Kong, "Li-ion battery fire hazards and safety strategies," *Energies*, vol. 11, no. 9, pp. 2191, Sept. 2018.

[11] R. Kantharaj and A. M. Marconnet, "Heat generation and thermal transport in lithium-ion batteries: a scale-bridging perspective," *Nanoscale and Microscale Thermophysical Engineering*, vol. 23, no. 2, pp. 128-156, Apr. 2019.

[12] R. Srinivasan, M. E. Thomas, M. B. Airola *et al.*, "Preventing cell-to-cell propagation of thermal runaway in lithium-ion batteries," *Journal of the Electrochemical Society*, vol. 167, no. 2, pp. 1-6, Feb. 2020.

[13] H. Zhang, F. Mollet, C. Saudemont *et al.*, "Experimental validation of energy storage system management strategies for a local DC distribution system of more electric aircraft," *IEEE Transactions on Industrial Electronics*, vol. 57, no. 12, pp. 3905-3916, Mar. 2010.

[14] D. Wu, R. Todd, and A. J. Forsyth, "Adaptive rate-limit control for energy storage systems," *IEEE Transactions on Industrial Electronics*, vol. 62, no. 7, pp. 4231-4240, Dec. 2014.

[15] P. Sharma, "Closed loop controlled boost converter using a pid controller for solar wind power system installation," *International Journal of Engineering & Technology*, vol. 7, no. 2.8, pp. 255-260, Mar. 2018.

[16] A. Berrueta, A. Ursua, I. S. Martin *et al.*, "Supercapacitors: electrical characteristics, modeling, applications, and future trends," *IEEE Access*, vol. 7, pp. 50869-50896, Apr. 2019.

[17] C. Xiang, Y. Wang, S. Hu *et al.*, "A new topology and control strategy for a hybrid battery-ultracapacitor energy storage system," *Energies*, vol. 7, no. 5, pp. 2874-2896, May 2014.

[18] M. Ortúzar, J. Moreno, and J. Dixon, "Ultracapacitor-based auxiliary energy system for an electric vehicle: implementation and evaluation," *IEEE Transactions on Industrial Electronics*, vol. 54, no. 4, pp. 2147-2156, Jul. 2007.

[19] K. Kim, J. An, K. Park *et al.*, "Analysis of a supercapacitor/battery hybrid power system for a bulk carrier," *Applied Sciences*, vol. 9, no. 8, pp. 1547, Jan. 2019.

[20] S. D. Vidhya and M. Balaji, "Modelling, design and control of a light electric vehicle with hybrid energy storage system for Indian driving cycle," *Measurement and Control*, vol. 52, no. 9-10, pp. 1420-1433, Nov. 2019.

[21] V. Mali and B. Tripathi, "Thermal and economic analysis of hybrid energy storage system based on lithium-ion battery and supercapacitor for electric vehicle application," *Clean Technologies and Environmental Policy*, vol. 23, pp. 1135-1150, May 2021.

[22] S. Charles, C. Fredrick, K. Gopinath *et al.*, "Design and development of an extended range electric hybrid scooter," *Engineering Science and Technology*, vol. 2, pp. 196-203, Jan. 2012.

[23] Kurtus R. (2018, May). Coefficient of rolling friction. [Online]. Available: https://www. school-for- champions. com/science/friction_rolling. htm#.WwPFJIq-nIU

[24] Indiamart. (2018, May). Tail light for bike. [Online]. Available: https://www.indiamart.com/proddetail/tail-light-for-bike-8928499588.html

[25] D. Chandran and M. Joshi, "Electric vehicles and driving range extension-a literature review," *Advances in Automobile Engineering*, vol. 2, no. 5, pp. 1-10, Jan. 2016.

[26] X. Liu, Q. Zhang, and C. Zhu, "Design of battery and ultracapacitor multiple energy storage in hybrid electric vehicle," in *Proceedings of 2009 IEEE Vehicle Power and Propulsion Conference*, Dearborn, USA, Sept. 2009, pp. 1395-1398.

[27] C. Xiang, Y. Wang, S. Hu *et al.*, "A new topology and control strategy for a hybrid battery-ultracapacitor energy storage system," *Energies*, vol. 7, no. 5, pp. 2874-2896, Apr. 2014.

[28] S. Tie and C. Tan, "A review of energy sources and energy management system in electric vehicles," *Renewable and Sustainable Energy Reviews*, vol. 20, pp. 82-102, Apr. 2013.

[29] M. Yassine and D. Fabris, "Performance of commercially available supercapacitors," *Energies*, vol. 10, no. 9, pp. 1-12, Sept. 2017.

[30] A. B. Cultura and Z. M. Salameh, "Modeling, evaluation and simulation of a supercapacitor module for energy storage application," in *Proceedings of International Conference on Computer Information Systems and Industrial Applications*, Bangkok, Thailand, Jun. 2015, pp.

876-882.

[31] D. L. Chapman, "Li–a contribution to the theory of electrocapillarity," *The London, Edinburgh, and Dublin Philosophical Magazine and Journal of Science*, vol. 25, no. 148, pp. 475-481, Apr. 1913.

[32] J. Deng, J. Li, S. Song *et al.*, "Electrolyte-dependent supercapacitor performance on nitrogen-doped porous bio-carbon from gelatin," *Nanomaterials*, vol. 10, no. 2, pp. 1-23, Feb. 2020.

[33] D. K. Kampouris, "A new approach for the improved interpretation of capacitance measurements for materials utilised in energy storage," *RSC Advances*, vol. 5, no. 17, pp. 12782-12791, Jan. 2015.

[34] W. Waag, S. Käbitz, and D. U. Sauer, "Experimental investigation of the lithium-ion battery impedance characteristic at various conditions and aging states and its influence on the application," *Applied Energy*, vol. 102, pp. 885-897, Feb. 2013.

[35] A. Hammar, "Study of accelerated aging of supercapacitors for transport applications," *IEEE Transactions on Industrial Electronics*, vol. 57, no. 12, pp. 3972-3979, Apr. 2010.

[36] P. Bhatnagar and F. Beyette, "Microcontroller-based electrochemical impedance spectroscopy for wearable health monitoring systems," in *Proceedings of 2015 IEEE 58th International Midwest Symposium on Circuits and Systems (MWSCAS)*, Fort Collins, USA, Aug. 2015, pp. 1-4.

[37] M. Tutuianu, "Development of the world-wide harmonized light duty test cycle (WLTC) and a possible pathway for its introduction in the European legislation," *Transportation Research Part D: Transport and Environment*, vol. 40, pp. 61-75, Oct. 2015.

[38] Y. Ji and C. Wang, "Heating strategies for Li-ion batteries operated from subzero temperatures," *Electrochimica Acta*, vol. 107, pp. 664-674, Sept. 2013.

[39] Y. Miao, P. Hynan, A. von Jouanne *et al.*, "Current Li-ion battery technologies in electric vehicles and opportunities for advancements," *Energies*, vol. 12, no. 6, pp. 1-20, Jan. 2019.

[40] X. Peng, S. Chen, A. Garg *et al.*, "A review of the estimation and heating methods for lithium-ion batteries pack at the cold environment," *Energy Science & Engineering*, vol. 7, no. 3, pp. 645-662, Jun. 2019.

[41] S. R. Soni, C. D. Upadhyay, and H. Chandwani, "Analysis of battery-super capacitor based storage for electrical vehicle," in *Proceedings of 2015 International Conference on Energy Economics and Environment (ICEEE)*, Greater Noida, India, Mar. 2015, pp. 1-7.

[42] M. Mousavi, P. M. Shabestari, and A. Mehrizi-Sani, "Analysis and output voltage control of a high-efficiency converter for DC microgrids," in *Proceedings of IECON 2018–44th Annual Conference of the IEEE Industrial Electronics Society*, Washington DC, USA, Oct. 2018, pp. 1029-1034.

[43] S. Bhoyate, C. K. Ranaweera, C. Zhang *et al.*, "Eco-friendly and high performance supercapacitors for elevated temperature applications using recycled tea leaves," *Global Challenges*, vol. 1, no. 8, p.1700063, Nov. 2017.

Vima Mali received the B.E. degree from Visvesvaraya Technological University, Belgaum, Karnataka, in 2009, and the M.E. degree from Davangere University, Tholahunase, Karnataka, in 2011. She is pursuing the Ph.D. degree in the area of supercapacitor based hybrid energy storage system for electric vehicle application at Pandit Deendayal Petroleum University (PDPU), Gandhinagar, India. And she is currently working as an Assistant Professor at Department of Electrical Engineering, School of Technology, PDPU. She is a Life Member of the Institution of Engineers of India. Her research interests include hybrid electrical energy storage system and thermal management in electric vehicle.

Brijesh Tripathi received the B.Sc. and M.Sc. degrees from C.S.J.M. University, Kanpur, India, in 2003 and 2005, respectively. He received the Ph. D. degree from Pandit Deendayal Petroleum University (PDPU), Gandhinagar, India, in 2014. He is currently working as an Assistant Professor at Department of Physics, School of Technology, PDPU. He is a Life Member of Solar Energy Society of India (SESI) and Indian Society for Technical Education (ISTE). His research interests include thin-film deposition technologies through various vacuum and non-vacuum techniques. His research interests include solar photovoltaic, electronic device, electro-chemistry, and electric vehicle.